TOWARDS THE SPECTRAL RESTORATION OF SHADOWED AREAS IN HYPERSPECTRAL IMAGES BASED ON NONLINEAR UNMIXING

Guichen Zhang, Daniele Cerra, Rupert Müller

German Aerospace Center (DLR)
Remote Sensing Technology Institute (IMF)
82234 Wessling, Germany

ABSTRACT

This work proposes a new shadow restoration method for hyperspectral images based on nonlinear unmixing. A physical model is introduced to estimate the shadowed spectrum from a spectrum of the same material exposed to direct sunlight. By defining pure spectra receiving direct and indirect illumination as sunlit and shadowed endmembers, respectively, the proposed method estimates the abundance maps for both sunlit and shadowed endmembers pixelwise, taking into account nonlinear effects up to the second order, which are of particular importance in shadow areas. Subsequently, the spectrum of a pixel in a scene is restored by a linear combination of sunlit and shadowed endmembers. Experimental results show that shadowed spectra can be successfully recovered and their true reflectance better estimated. In addition, the proposed method solves shadow detection and restoration simultaneously, so that it does not need a shadows mask as an additional input.

Index Terms— shadow restoration, hyperspectral images, nonlinear spectral unmixing

1. INTRODUCTION

Hyperspectral imagery contains rich spectral information and its use in remote sensing applications has increased in recent years [1]. For the case of hyperspectral data acquired by airborne sensor, the high spatial resolution allows observing shadowed areas caused e.g. by buildings, trees, or clouds. Due to the lack of direct sun illumination, the reflectance estimated in shadowed pixels is not correct and leads to problems in image analysis [2]. Therefore, it would be desirable to derive the real reflectance for a material in the shadows before further analysis.

Ashton et al. [3] transformed hyperspectral reflectance data to hyperspherical coordinates in order to suppress the difference between shadowed and lighted pixels of the same material. Roussel et al. [4, 5, 6] assumed that the spectral angle between sunlit and shadow pixels for the same material is small. Yamazaki et al. [7] observed that the shadow effects depend on acquisition time and season of an image, casting conditions of the shadows, and wavelength. They computed a linear relationship between exposed and shadowed pixels for each band with the same material by using linear regression. Two models based on clear physical assumptions have also been proposed in ([2, 8]), where the authors modeled spectral radiance pixelwise based on the physics of the image processing chain. Pixels under direct sunlight are assumed to receive both direct sun illumination and irradiance from the sky, while shadowed pixels only receive irradiance from the sky. Lidar or DSM data were used to compute the casting conditions of shadows and the amount of sky directly visible from each pixel. In addition, spectral unmixing methods have been widely used to analyze elementary materials in hyperspectral images, and they allow multiple materials to be present in one pixel [1]. Traditional spectral unmixing methods [1] could fail when applied to shadowed areas. Liu et al. [9] proposed a shadow restoration method based on linear unmixing. A shadowed pixel is assumed to be a wavelength-dependent affine transformation of a pixel exposed to direct sunlight for a specific material. However, shadowed pixels contain nonlinear interactions which should not be omitted [10, 11], as their contribution becomes meaningful. Heylen et al. [10] proposed a nonlinear mixture model with a clear physical process to detect shadow pixels. Nascimento et al. [11] studied an example of dry grass shadowed by trees through a nonlinear mixture model. Shadow pixels were regarded as an endmember which was computed by multiplying the reflectance of the dry grass with the one related to the tree. To the best of our knowledge, current works about shadow restoration methods are still limited by the following aspects. Firstly, a shadow detection step is required before conducting shadow restoration, as a shadows mask is usually required as additional input. Secondly, the training samples should be manually selected. Finally, some methods, which are not based on physical interpretation, may lead to large spectral distortion between the restored spectra of shadowed pixels and the spectra of the corresponding sunlit pixels. In this work, we aim at dealing with airborne hyperspectral images and propose a shadow restoration method based on the nonlinear mixture model, under some physical assumptions. In our model, the shadow

detection step is naturally embedded, and endmembers must be manually selected. The results include abundance maps related to spectra belonging the same material under direct sunlight or in the shadows, nonlinearity parameters, and a restored hyperspectral image subset.

2. METHOD

According to [12], direct sunlight and diffused skylight are two major illumination sources for sunlit pixels (pixels exposed to direct sunlight). We neglect the latter for sunlit pixels in this paper, as it is significantly smaller. Besides, we assume that the targets on ground are Lambertian, and that both the incident direction of sunlight and the viewing direction of the sensor are constant across a small scene. Then, the reflectance of a sunlit pixel is written as:

$$r_l(\lambda) = \frac{\pi \cdot L_l(\lambda)}{E_{l(\lambda)}} \tag{1}$$

where $L_l(\lambda) = \frac{E_l(\lambda) \cdot r_l(\lambda)}{\pi}$ is the radiance of the sunlit pixel at wavelength λ, and E_l is the irradiance at the sunlit pixel at wavelength λ[1].

For shadowed pixels, two additional relevant illumination sources are diffused skylight and reflections from the surrounding objects. The atmospheric correction step does not process sunlit and shadow pixels separately, as it adopts the same workflow for both. The observed reflectance for a shadow pixel can be written as:

$$r_s(\lambda) = \frac{\pi \cdot L_s(\lambda)}{E_l(\lambda)} + \frac{\pi \cdot L'_s(\lambda)}{E_l(\lambda)} \tag{2}$$

where $L_s(\lambda) = \frac{E_s(\lambda) \cdot r_l(\lambda)}{\pi}$ is the radiance of the shadowed pixel contributed by the linear part at wavelength λ, $L'_s(\lambda)$ is the radiance of the shadowed pixel contributed by nonlinear effects at wavelength λ, and $E_s(\lambda)$ is the diffuse skylight at wavelength λ.

The problem becomes then how to model $L'_s(\lambda)$ in equation (2). Modeling nonlinear effects for spectral unmixing has been explored for decades. Recent reviews on nonlinear spectral unmixing could be found in [1, 13, 14]. In this paper, we model $L'_s(\lambda)$ using a second-order polynomial with a free parameter b [15]. This model considers self-reflections of endmembers and contains only one scaling parameter. As diffused skylight is the only illumination source, the indirect light source of multi-reflections is diffused skylight.

$$L'_s(\lambda) = \frac{b \cdot E_s(\lambda) \sum_{i=1}^{p} \sum_{j=1}^{p} a_i \cdot a_j \cdot r_{l,i}(\lambda) \cdot r_{l,j}(\lambda)}{\pi} \tag{3}$$

where b is a scaling parameter, $E_s(\lambda)$ is diffused skylight at wavelength λ, p is the number of materials (endmember) in one pixel, $r_{l,i}(\lambda)$ is the i-th reflectance of sunlit material (endmember) at wavelength λ, a_i is the i-th abundance corresponding to $r_{l,i}$.

After combining equation (1-3), r_s can be written as:

$$r_s(\lambda) = \frac{E_s(\lambda)}{E_l(\lambda)} \cdot r_l + \frac{E_s(\lambda)}{E_l(\lambda)} \cdot b \cdot \sum_{i=1}^{p} \sum_{j=1}^{p} a_i \cdot a_j \cdot r_{l,i}(\lambda) \cdot r_{l,j}(\lambda) \tag{4}$$

Here, $\frac{E_s(\lambda)}{E_l(\lambda)}$ could be interpreted as the ratio between diffused skylight and sun's emissions. If images are acquired under a clear sky, rayleigh scattering could be seen as the main contribution of atmospheric particles, and $\frac{E_s(\lambda)}{E_l(\lambda)}$ preserves a positive correlation with an exponential decreasing function λ^{-4}[16, 17]:

$$\frac{E_s(\lambda)}{E_l(\lambda)} = F \cdot \frac{\lambda^{-}4}{\sum_{c=1}^{B} \lambda_c^{-}4} \tag{5}$$

where λ is a wavelength, λ_c the c-th central wavelength for a band of the input hyperspectral image, B the total number of bands of the input image, and F a scaling factor.

By combining equation (4) and (5), we have:

$$\begin{aligned} r_s(\lambda) = {} & F \cdot \frac{\lambda^{-}4}{\sum_{c=1}^{B} \lambda_c^{-}4} \cdot r_l(\lambda) + \\ & F \cdot \frac{\lambda^{-}4}{\sum_{c=1}^{B} \lambda_c^{-}4} \cdot b \cdot \sum_{i=1}^{p} \sum_{j=1}^{p} a_i \cdot a_j \cdot r_{l,i}(\lambda) \cdot r_{l,j}(\lambda) \end{aligned} \tag{6}$$

So far, shadowed reflectance has been modeled by using sunlit reflectance at the same wavelength λ, together with abundances and estimated parameters. We further extend equation (6) to vector form to solve all wavelengths together, and construct a nonlinear mixture model to allow more materials to be present in one pixel, and to be only partially exposed to direct sunlight.

Here $\boldsymbol{e\_l_i}$ is the i-th sunlit endmember containing B spectral bands, where $i = 1, 2, ...p$, p is the total number of endmembers, a_l_i the i-th abundance corresonding to the i-th sunlit endmember, and a_s_i the i-th abundance corresponding to the the i-th shadowed endmember. Given an i-th sunlit endmember $\boldsymbol{e\_l_i}$, a corresponding shadowed endmember $\boldsymbol{e\_s_i}$ can be written as:

$$\begin{aligned} \boldsymbol{e\_s_i} = {} & F \cdot \frac{\boldsymbol{\lambda^{-}4}}{\sum_{c=1}^{B} \boldsymbol{\lambda_c^{-}4}} \cdot \boldsymbol{e\_l_i} + \\ & F \cdot \frac{\boldsymbol{\lambda^{-}4}}{\sum_{c=1}^{B} \lambda_c^{-}4} \cdot b \cdot \sum_{i=1}^{p} \sum_{j=1}^{p} a_i \cdot a_j \cdot \boldsymbol{e\_l_i} \cdot \boldsymbol{e\_l_j} \end{aligned} \tag{7}$$

Then both $\boldsymbol{e\_l_i}$ and $\boldsymbol{e\_s_i}$ can be regarded as endmembers. Additionally, we model nonlinear effects of sunlit endmembers $\boldsymbol{e\_l_i}$ through a second-order polynomial [15]. Thus, for

[1] λ is a given wavelength in this paper unless otherwise noted

one pixel $\boldsymbol{x}$ with B spectral bands we have:

$$\begin{aligned}\boldsymbol{x} = &\sum_{i=1}^{p} a\_l_i \cdot \boldsymbol{e\_l_i} + \sum_{i=1}^{p} a\_s_i \cdot F \cdot \frac{\boldsymbol{\lambda^{-4}}}{\sum_{c=1}^{B} \boldsymbol{\lambda_c^{-4}}} \cdot \boldsymbol{e\_l_i} \\ &+ F \cdot \frac{\boldsymbol{\lambda^{-4}}}{\sum_{c=1}^{B} \boldsymbol{\lambda_c^{-4}}} \cdot b \cdot \sum_{i=1}^{p}\sum_{j=1}^{p} a\_s_i \cdot a\_s_j \cdot \boldsymbol{e\_l_i} \cdot \boldsymbol{e\_l_j} \\ &+ b \cdot \sum_{i=1}^{p}\sum_{j=1}^{p} a\_l_i \cdot a\_l_j \cdot \boldsymbol{e\_l_i} \cdot \boldsymbol{e\_l_j}\end{aligned} \quad (8)$$

where $\sum_{i=1}^{p} a\_l_i + a\_s_i = 1$, $a\_l_i \geq 0$, and $a\_s_i \geq 0$.

As a_s_i and a_l_i are the abundances of shadowed and sunlit endmembers for the same material, the shadow restoration result $\boldsymbol{x_{restore}}$ of pixel $\boldsymbol{x}$ with B spectral bands is computed by:

$$\boldsymbol{x_{restore}} = \sum_{i=1}^{p} (a\_l_i + a\_s_i) \cdot \boldsymbol{e_i} \quad (9)$$

3. DATA

We used a subset from an airborne hyperspectral image acquired over Oberpfaffenhofen, Bavaria, Germany (Fig. 1) with a HySpex VNIR sensor flying at an altitude of 1615 m, resulting in a spatial resolution of 0.7 m. The image comprises 160 spectral bands ranging from 416 nm to 988.4 nm. The image was atmospherically corrected, and ground reflectance data were used in this paper. We have manually selected 6 (sunlit) endmembers from the image: grass, tree, highway, road, roof1, and roof2 (see Fig. 1).

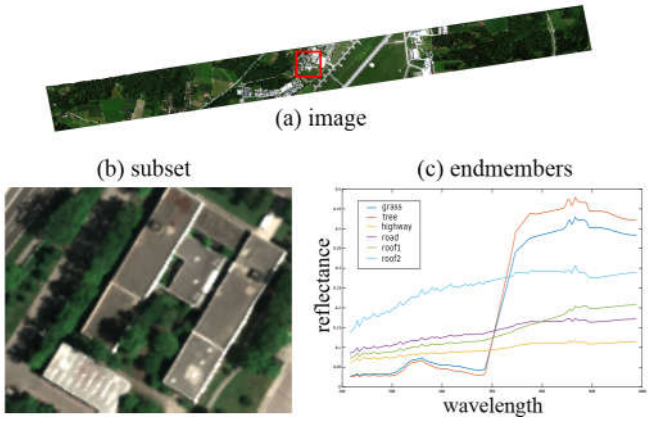

Fig. 1. Hpyerspectral image with manually selected endmembers.

4. RESULTS

In the reported experiments, our inputs were the hyperspectral image and the manually selected endmembers introduced in section 3. Furthermore, the spectral unmixing process assumes two constraints on the abundances, i.e., the abundance non-negativity constraint (ANC) and the abundance sum-to-one constraint (ASC) [13]. The outputs of the proposed method were the abundance maps of sunlit and shadowed endmembers, and two scaling factors (see Fig. 2).

We have found out that it is difficult to estimate abundances of shadowed endmembers accurately when their corresponding sunlit endmembers are very similar, as reflectance values decrease significantly for shadowed pixels, and the noise plus the variations in illumination conditions may be larger than the spectral differences between the similar classes. When two materials are similar in sunlit condition, their difference is negligible in the shadowed condition. This phenomenon happens between grass and tree and also comes out among highway, road, and roofs.

Therefore, it is reasonable to combine abundance values of shadowed endmembers by summing them, when their corresponding sunlit endmembers are highly similar. We summed up the abundance maps of shadowed grass and shadowed tree as shadowed vegetation, and the abundance maps of shadowed highway, shadowed road, and shadowed roofs as shadowed asphalt.

Furthermore, the spectra of shadowed pixels where asphalt was shadowed by tree exhibited an obvious red edge feature due to nonlinear scattering effects. Such feature was less evident than in shadowed vegetation. Thus, normalized difference vegetation index (NDVI) was applied in order to separate shadowed vegetation from shadowed asphalt through thresholding (the threahold was empirically set as 0.75 in this paper).

Fig. 2 (a)-(f) presents the abundance maps of sunlit endmembers, while Fig. 2 (g)-(h) shows the abundances of shadowed vegetation and asphalt. After comparing abundance maps with the input image, it has been observed that our proposed method has successfully extracted abundance values of sunlit and shadowed endmembers.

In addition, F and b maps are reported in Fig. 2 (i) and (k), respectively. The former, which is a scaling factor of Rayleigh scattering, is larger for sunlit pixels and lower for shadow pixels. The latter, which is a scaling factor in the proposed nonlinear mixture model, is much higher for shadow pixels.This indicates that nonlinear effects have a high impact on shadow pixels and are important for shadow analysis.

Fig. 3 reports a visual comparison of the original image with the restored one in four regions, in which road, grass, or roof were shadowed by trees. The proposed method successfully restored shadow pixels. In order to assess if shadow restoration results could introduce spectral distortions among all spectral bands, we compare in Fig. 3 the restored spectrum ("restored") with three other spectra selected respectively from the input shadow pixel ("observed" in the legend), the endmember illuminated from direct sunlight corresponding to the input shadow pixel ("endmember" in the legend),

and a spectrum from the same material under direct sunlight, located in the neighborhood of the shadowed pixel ("sunlit" in the legend). Ideally, the spectra noted as "endmember" and "sunlit" should be very similar, but they are different in reality due to interclass spectral variability. In this experiment, we regarded both the spectra "endmember" and "sunlit" as true spectra of the material exposed to direct sunlight. In Fig. 3, the spectrum of an input shadowed pixel ("observed") is not simply divided by a scaling factor with respect to the spectrum of the same material exposed to direct sunlight, as both Rayleigh scattering and nonlinear effects have a large impact on the spectral features and are wavelength dependent. After applying our proposed method, the restored spectra ("restored") exhibit similar spectral characteristics to the "sunlit" and "endmember" spectra, indicating that our shadow removal results are not only visually convincing in a true color combination of the image subset, but more importantly keep unaltered the main spectral features of the targets of interest.

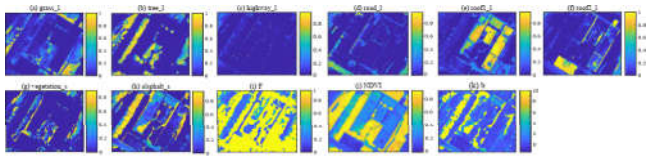

Fig. 2. Estimated abundances and parameters. Top row: abundances for endmembers exposed to sunlight. Bottom row, from left to right: abundances of shadowed vegetation and asphalt, Rayleigh scaling factor F, and nonlinear scaling factor for PPNM b.

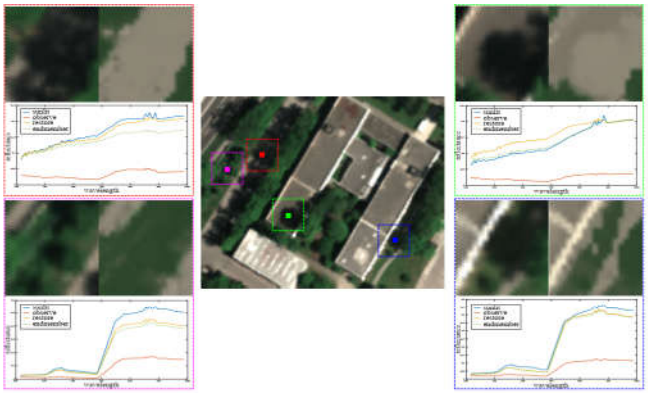

Fig. 3. Results for spectral reconstruction in shadowed areas. Center: true color subset of hyperspectral HySpex image acquired over DLR premises in Oberpfaffenhofen, Germany. Four corners: detail of the image subset (left), its reconstruction image (right), spectral comparison of shadowed material, restored spectrum, spatially close pixel exposed to sunlight, and relative endmember exposed to sunlight.

5. CONCLUSION

This paper proposes a novel shadow restoration method for hyperspectral images based on the nonlinear mixture model, based on physical assumptions of the different indirect illumination sources which are relevant in shadowed areas. The proposed method achieves satisfying results on a high resolution hyperspectral dataset. The restored shadowed areas are visually convincing, and their spectral information presents only limited distortion.

Future work includes the development of a fully automatic shadow restoration framework by embedding an automatic endmember extraction algorithm, and the validation on different and larger hyperspectral subsets.

6. REFERENCES

[1] Nicolas Dobigeon, Jean-Yves Tourneret, Cédric Richard, José Carlos M Bermudez, Stephen McLaughlin, and Alfred O Hero, "Nonlinear unmixing of hyperspectral images: Models and algorithms," *IEEE Signal Processing Magazine*, vol. 31, no. 1, pp. 82–94, 2014.

[2] Qiang Zhang, V Paúl Pauca, Robert J Plemmons, and D Dejan Nikic, "Detecting objects under shadows by fusion of hyperspectral and lidar data: A physical model approach," in *2013 5th Workshop on Hyperspectral Image and Signal Processing: Evolution in Remote Sensing (WHISPERS)*. IEEE, 2013, pp. 1–4.

[3] Edward A Ashton, Brian D Wemett, Robert A Leathers, and Trijntje V Downes, "A novel method for illumination suppression in hyperspectral images," in *Algorithms and Technologies for Multispectral, Hyperspectral, and Ultraspectral Imagery XIV*. International Society for Optics and Photonics, 2008, vol. 6966, p. 69660C.

[4] Guillaume Roussel, Christiane Weber, Xavier Ceamanos, and Xavier Briottet, "A sun/shadow approach for the classification of hyperspectral data," in *2016 8th Workshop on Hyperspectral Image and Signal Processing: Evolution in Remote Sensing (WHISPERS)*. IEEE, 2016, pp. 1–5.

[5] Fatih Omruuzun, Didem Ozisik Baskurt, Hazan Daglayan, and Yasemin Yardimci Cetin, "Shadow removal from vnir hyperspectral remote sensing imagery with endmember signature analysis," in *Next-Generation Spectroscopic Technologies VIII*. International Society for Optics and Photonics, 2015, vol. 9482, p. 94821F.

[6] Moussa Sofiane Karoui and Khelifa Djerriri, "A new unmixing-based approach for shadow correction of hy-

perspectral remote sensing data," in *IGARSS 2018-2018 IEEE International Geoscience and Remote Sensing Symposium*. IEEE, 2018, pp. 2725–2728.

[7] Fumio Yamazaki, Wen Liu, and Makiko Takasaki, "Characteristics of shadow and removal of its effects for remote sensing imagery," in *2009 IEEE International Geoscience and Remote Sensing Symposium*. IEEE, 2009, vol. 4, pp. IV–426.

[8] Ola Friman, Gustav Tolt, and Jörgen Ahlberg, "Illumination and shadow compensation of hyperspectral images using a digital surface model and non-linear least squares estimation," in *Image and Signal Processing for Remote Sensing XVII*. International Society for Optics and Photonics, 2011, vol. 8180, p. 81800Q.

[9] Yi Liu, José Bioucas-Dias, Jun Li, and Antonio Plaza, "Hyperspectral cloud shadow removal based on linear unmixing," in *2017 IEEE International Geoscience and Remote Sensing Symposium (IGARSS)*. IEEE, 2017, pp. 1000–1003.

[10] Rob Heylen, Vera Andrejchenko, Zohreh Zahiri, Mario Parente, and Paul Scheunders, "Nonlinear hyperspectral unmixing with graphical models," *IEEE Transactions on Geoscience and Remote Sensing*, 2019.

[11] José MP Nascimento and José M Bioucas-Dias, "Nonlinear mixture model for hyperspectral unmixing," in *Image and Signal Processing for Remote Sensing XV*. International Society for Optics and Photonics, 2009, vol. 7477, p. 74770I.

[12] John R Schott, *Remote sensing: the image chain approach*, Oxford University Press on Demand, 2007.

[13] Rob Heylen, Mario Parente, and Paul Gader, "A review of nonlinear hyperspectral unmixing methods," *IEEE Journal of Selected Topics in Applied Earth Observations and Remote Sensing*, vol. 7, no. 6, pp. 1844–1868, 2014.

[14] Yannick Deville and Leonardo Tomazeli Duarte, "An overview of blind source separation methods for linear-quadratic and post-nonlinear mixtures," in *International Conference on Latent Variable Analysis and Signal Separation*. Springer, 2015, pp. 155–167.

[15] Yoann Altmann, Abderrahim Halimi, Nicolas Dobigeon, and Jean-Yves Tourneret, "Supervised nonlinear spectral unmixing using a postnonlinear mixing model for hyperspectral imagery," *IEEE Transactions on Image Processing*, vol. 21, no. 6, pp. 3017–3025, 2012.

[16] Mark Cameron and Lalit Kumar, "Diffuse skylight as a surrogate for shadow detection in high-resolution imagery acquired under clear sky conditions," *Remote Sensing*, vol. 10, no. 8, pp. 1185, 2018.

[17] Pat S Chavez Jr, "An improved dark-object subtraction technique for atmospheric scattering correction of multispectral data," *Remote sensing of environment*, vol. 24, no. 3, pp. 459–479, 1988.